JOURNAL OF MECHANICAL AND TRANSPORT ENGINEERING
Vol. 68, no. 3 2016
DOI 10.21008/j.2449-920X.2016.68.3.05

Dominik WOJTKOWIAK*
Krzysztof TALAŚKA*
Ireneusz MALUJDA*
(Paper received on 02.06.2016, Paper accepted for publication on 07.07.2016)

COMPUTER ANALYSIS OF INSECT-LIKE ROBOT LEG STRUCTURE – PART 1 – STATIC FINITE-ELEMENT ANALYSIS

The purpose of this paper is to present the relationship between loading of the leg and the posture of an insect-like robot determined through computer simulation study. It presents the results of a static FEM analysis of a 3D robotic leg model performed using Abaqus 6.13. It also presents the kinematic structure of an insect-like walking robot capable of object manipulation.

Keywords: walking robot, walking machine, hexapod, quadruped, robotic leg

1. INTRODUCTION

Insects are the most typical inspiration for the design of hexapods – the most common walking robots. Insects have only three pairs of legs. Their bodies are divided into a smaller number of parts as compared to other arthropods: arachnids and crustaceans which have four and five pairs of legs respectively. Insects have a three-part body with chitinous outer covering and one pair of legs per segment of the body. The feature specific to insects is that they do not incline their bodies during movement as other anthropods. Their legs have a much more complex structure, as compared to other anthropods due to a variety of functions they need to perform. They are used not only to walk but also to jump, swim, catch prey, gather food and can be equipped with various receptors designed to receive information from the environment [Friedrich and Zielińska 2004, Lewinger Branicky and Quinn 2005, Wojtkowiak 2015, Zielińska 2014].

* Chair of Basics of Machine Design, Poznan University of Technology.

The insect leg schematic is presented in Fig. 1. It is built of long segments linked by joints. These segments are called the femur, the trochanter, the coxa, the tibia, the tarsus. The trochanter is a short segment linked by joints with the femur and the tibia allowing rotation of the coxa in relation to the lower part of the leg. The tursus can be compared to a foot of a man. It is elastic and often tipped with tarsal claws whose function is to dampen shocks and grip the substrate (soil). Moreover, it can be coated with a sticky substance to enhance friction. The insect legs are covered with scales making up the exoskeleton which are thinner and less rigid at joints. Insects can generate a multitude of walking patterns. Fig. 1 presents also the most typical postures assumed by insects [Friedrich and Zielińska 2004, Morecki and Knapczyk 1999, Wojtkowiak 2015, Zielińska 2014].

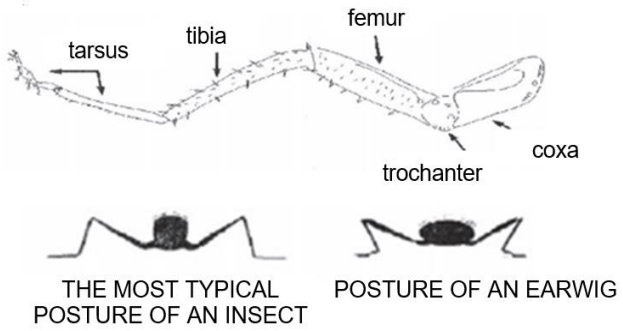

Fig. 1. Schematics of insect leg and typical postures [Friedrich and Zielińska 2004]

2. THE DESIGN AND CONFIGURATIONS OF AN INSECT-LIKE WALKING ROBOT

Fig. 2 presents a kinematic diagram of an insect-like walking robot. It has a three-part body comprising front body segment K1, middle body segment K2 and rear body segment K3. Only one pair of legs is attached to each segment (with the left leg marked L and the right marked P). Owing to joints between the body segments it is possible to obtain two different configurations: HEXAPOD and QUADRUPED. In this way the construction combines the capabilities of six- and four-legged robots. The front body segment K1 together with legs L1 and P1 makes up the locomotion and manipulation system. Conversely, the remaining body segments K2 and K3 and the limbs attached to them are designed to generate walking motion only.

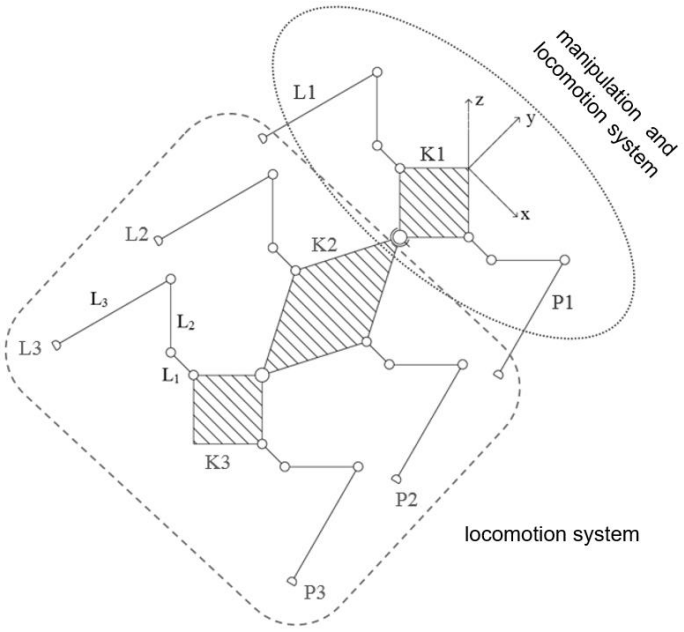

Fig. 2. Kinematic diagram of an insect-like walking robot: L1, L2, L3 – limbs on the left-hand side, P1, P2, P3 – limbs on the right hand side, K1 – front body segment, K2 – middle body segment, K3 – rear body segment, L_1, L_2, L_3 – links making up the limb

The HEXAPOD configuration (Fig. 3) in which the robot walks on six legs is the main body configuration. In this configuration the robot's capabilities are limited to locomotion. The merit of this configuration is a highly stable motion and a higher speed attainable by the robot increased by zigzag motion produced by employing the rotational degree of freedom about the vertical axis of both the joints of the body.

In the alternative QUADRUPED configuration (Fig. 4) the robot uses four limbs to move and the two front limbs to manipulate objects. Transformation from hexapod to quadruped configuration is possible owing to class 4 kinematic pair created by articulated joint between the front body segment K1 and middle body segment K2 allowing for rotation about the horizontal axis *x* and the vertical axis *z* (Fig. 2). Rotation of the body about the horizontal axis lifts the front body segment, as needed to perform the manipulation function by the manipulation and locomotion system. Rotation of the front body segment about the vertical axis extends the working space during manipulation. An additional advantage of such configuration is easier overcoming of obstacles.

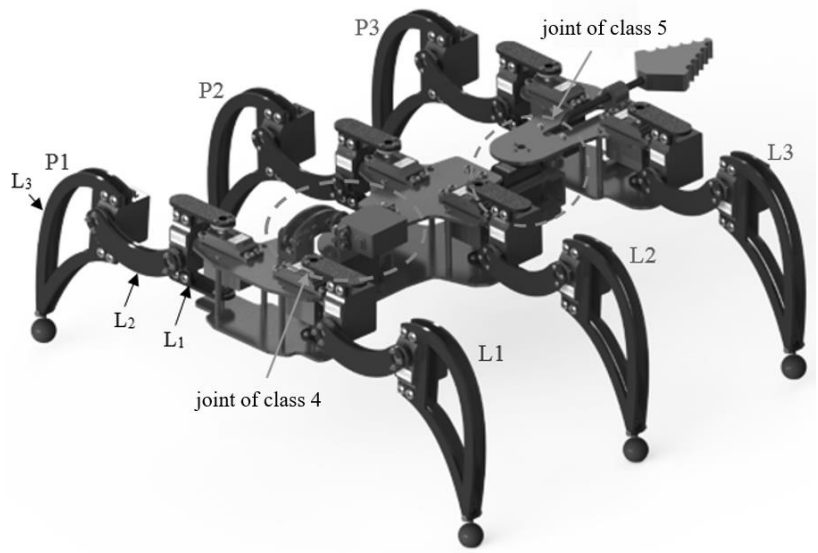

Fig. 3. Walking robot with HEXAPOD configuration: L1, L2, L3 – limbs on the left-hand side, P1, P2, P3 – limbs on the right hand side, K1 – front body segment, K2 – middle body segment, K3 – rear body segment, L_1, L_2, L_3 – links

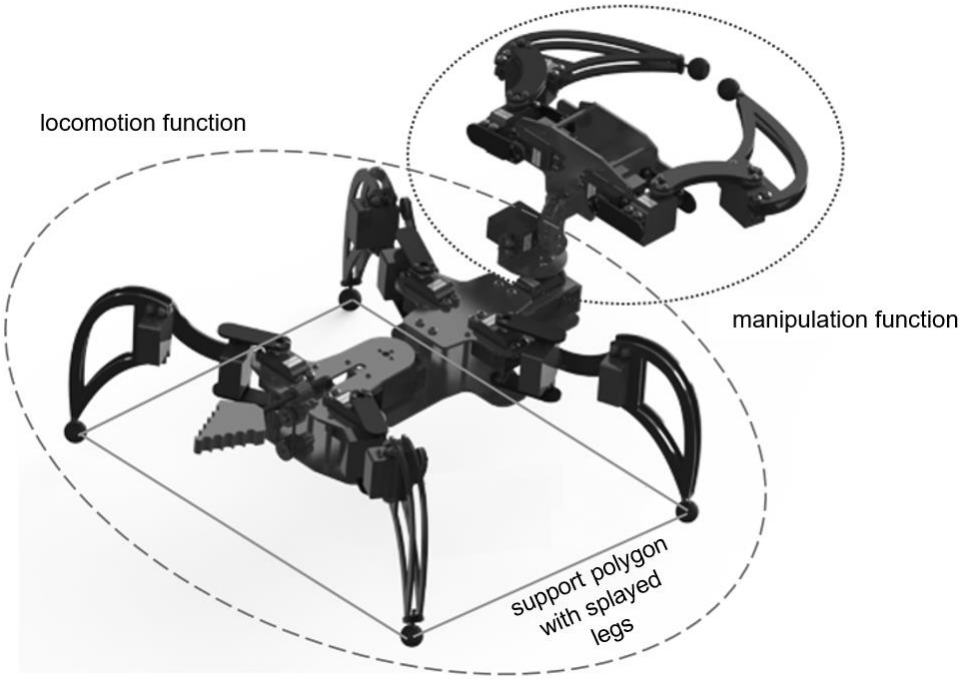

Fig. 4. Walking robot with QUADRUPED configuration

3. DESIGN OF THE WALKING ROBOT LEG

Irrespective of the walking machine configuration the main element performing a given function is the robotic leg called pedipulator (Fig. 5). Each limb is built of three links: L_1 – 35 mm long, L_2 – 80 mm long and L_3 – 140 mm long. The robotic leg is an open kinematic chain with each link connected with the preceding link with an articulated joint permitting rotation about horizontal axis making up kinematic pairs of class 5. Link L_1 is coupled with the robot body by an articulated joint permitting rotation about vertical axis and in this way making up kinematic pair of class 5. Link L_3 is ended with the foot. All the three links are situated in a single plane called „leg plane". The geometry of each of the three links is based on a bent crank or a pair of curved cranks connected by the driving mechanisms. Proportions other than defined by the insect model found in literature [1] were also applied. This resulted in obtaining a compact construction without compromising the working space needed to perform the intended functions and fitted with the necessary accessories.

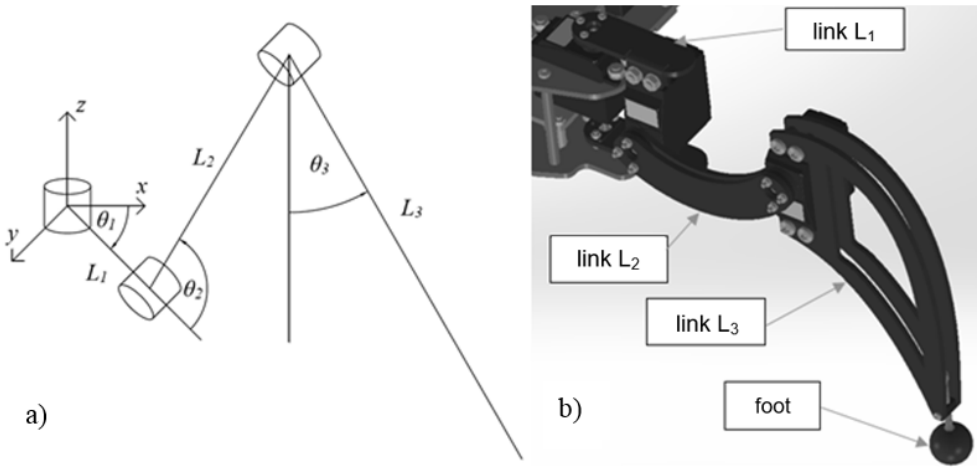

Fig. 5. Walking robot leg: a) kinematic schematic, b) 3D model

The angle of revolution of link L_1 about the vertical axis z (angle θ_1) determines the step length and the angles of rotation of links L_2 and L_3 about the axes perpendicular to the leg plane (angles θ_2 and θ_3) determine the robot's posture. The leg posture is understood as a set of kinematic configurations with a precisely determined range of change of the generalised co-ordinates [5]. The study presented in the further part of this paper concerns the effect of the robot's posture on the stresses generated in the respective links of the robot leg and the displacements.

4. PEDIPULATOR STATIC STRENGTH ANALYSIS USING FINITE ELEMENT METHOD

4.1. Experimental procedure

The static FEM analysis was performed with Abaqus 6.13 software suite. Fig. 6 presents a 3D model used in the analysis and the obtained results are presented in Fig. 7, 8 and 9. Boundary conditions BC1 and BC2 were related to removing all the translational degrees of freedom from the joints on the cylindrical surfaces of the openings used to attach the leg to the body. With the solid model used in the analysis it was not necessary to remove the rotational degrees of freedom. The model was loaded with pressures Load1 and Load2 imposed by the foot spring on its fixing. The analysis was carried out for the worse case situation from the point of view of loading in which the robot is supported on three legs. Change of posture resulted from the change in angle θ_2 from –75° to 60° at 15° increments and with unchanging angle θ_3.

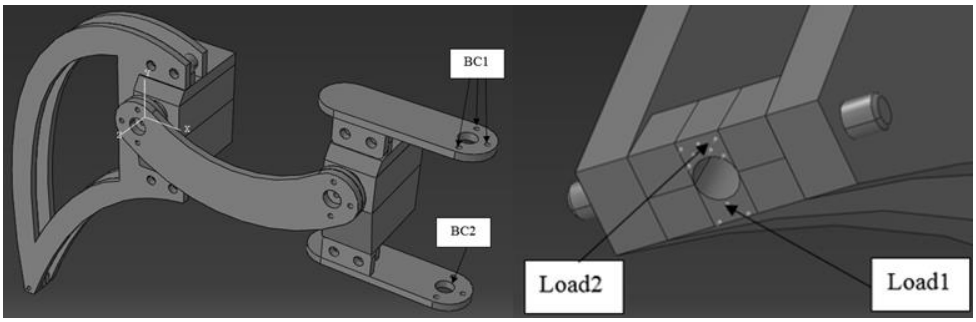

Fig. 6. 3D finite element model used in the static finite-element analysis

The output values for each posture were the equivalent von Mises stresses at the key points numbered 1 to 7 (see Fig. 7 and Fig. 8), displacements in the respective directions and the resultant displacement. The results obtained in this way are presented in Table 1. The key postures have been identified, for which the distribution of stresses in link L_2 being the most heavily loaded link are presented in Fig. 7 and Fig. 9. For the presented distributions the stress value was limited to 10 MPa for link L_2 and to 2 MPa for the remaining links. These limitations result from very high values of equivalent von Mises stresses in the servo horn, resulting from model simplification by introducing fixed connection between the servo horn surface and the edge of hole in link L_2. The results presented in 3.2 allow assessing both the magnitudes and the distribution of stresses in the respective links making up the leg of the walking robot under analysis.

4.2. Outcome of the Study

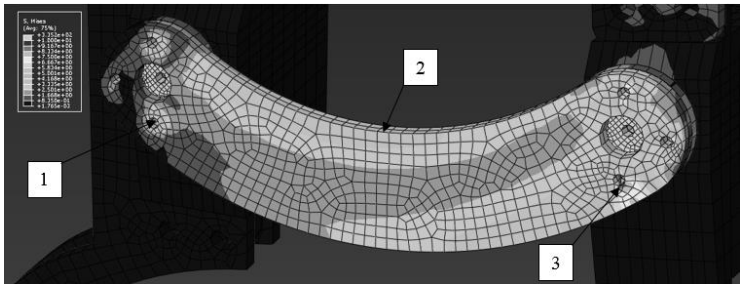

Fig. 7. Distribution of equivalent von Mises stresses for link L_2 and 0° posture (limit of 10 MPa)

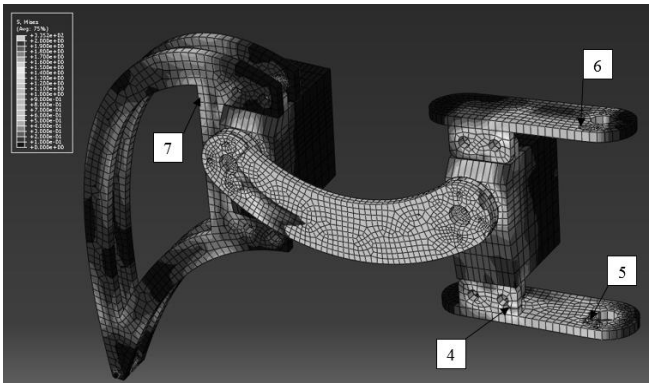

Fig. 8. Distribution of equivalent von Mises stresses in robot leg for 0° posture (limit of 2 MPa)

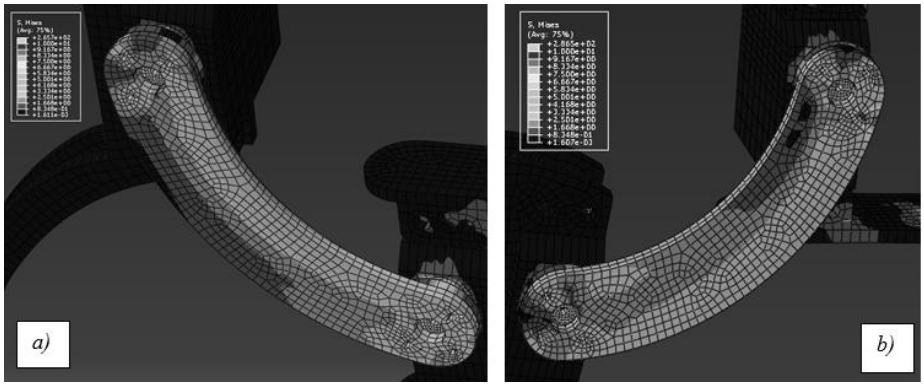

Fig. 9. Distribution of stresses for link L2 and postures a) 45° b) –45° (limit of 10 MPa)

Table 1

Values of equivalent von Mises stresses and displacements in the robot leg

θ_2	σ_1 [MPa]	σ_2 [MPa]	σ_3 [MPa]	σ_4 [MPa]	σ_5 [MPa]	σ_6 [MPa]	σ_7 [MPa]	U1 [mm]	U2 [mm]	U3 [mm]	U [mm]
–75°	21,21	5,33	11,43	1,52	2,57	3,88	0,88	–6,79	5,70	–12,03	14,87
–60°	13,43	5,61	14,79	1,59	2,60	3,90	0,88	–7,38	6,54	–11,44	14,99
–45°	15,13	5,02	14,2	1,66	2,61	3,92	0,88	–7,31	7,05	–10,07	14,17
–30°	16,30	4,88	13,09	1,72	2,63	3,94	0,88	–7,82	8,27	–9,29	14,56
–15°	17,19	4,23	11,54	1,76	2,64	3,95	0,88	–7,55	8,90	–8,09	14,07
0°	16,47	3,54	10,96	1,77	2,64	3,96	0,88	–6,53	8,66	–6,68	12,62
15°	17,70	3,98	10,65	1,76	2,64	3,95	0,88	–6,12	8,88	–6,24	12,32
30°	16,84	4,29	11,40	1,72	2,63	3,94	0,88	–5,22	8,25	–5,70	11,16
45°	15,53	4,47	11,78	1,66	2,61	3,92	0,88	–4,16	7,11	–5,17	9,59
60°	14,41	4,51	11,53	1,59	2,59	3,90	0,88	–3,84	6,64	–5,66	9,40

4.3. Analysis of Results

On the basis of the obtained distributions of stresses for the main configurations we can conclude as follows:

– for the 0° configuration the stresses on the inside and outside curves of the link are comparable while for the positive configuration their occurrence is limited to the inside curve of a smaller radius (point No. 2) and for the negative configuration they occur on both sides, more on the curve with a greater radius,

– concentration of stresses in the smaller radius curve for the positive configuration occurs on the surface more distant from the servo horns and for the opposite configuration stresses occur on the surface closer to them,

– for the negative configuration stresses for both curves occur at the opposite sides of the link – i.e. the link is subjected to both torsion and bending, different than in the other two cases in which it is subjected to bending only,

– the differences in stresses are found also between connection of L_2 links and the driven end of link L_3 (point No. 3) because the concentration of stresses occurs in the lower hole for positive angle and in upper hole for negative angle.

From the results presented in Table 1 we can see that the stresses at points 4–7 associated with links L_1 and L_3 do not change considerably when the robot posture is modified as described above. The changes in the values of the equivalent von Mises stresses at other points and in the displacements are presented in the graphs in Fig. 10 and Fig. 11 respectively. Displacement U1 along the axis transverse to the robot's walking direction is more or less symmetrical about the point for 0°. This means the displacements decrease with the increase in the value of positive

angle and increase with the increase in the value of negative angle. Vertical displacement U2 is symmetrical for positive and negative angles. The curve representing displacement U3 along the axis running in the walking direction is very irregular. Note that for positive angles the displacement values decrease only slightly with the decrease in the angle resulting in lowering of the robot posture. With increasing negative angle values resulting in increasing the ground clearance the displacement is that direction starts to increase rapidly. The U3 displacement is related to splaying of the whole leg away from the theoretical plane of movement of links L_2 and L_3. This could be avoided by increasing rigidity of the construction, yet this would increase the weight and the amount of energy needed to perform the movements.

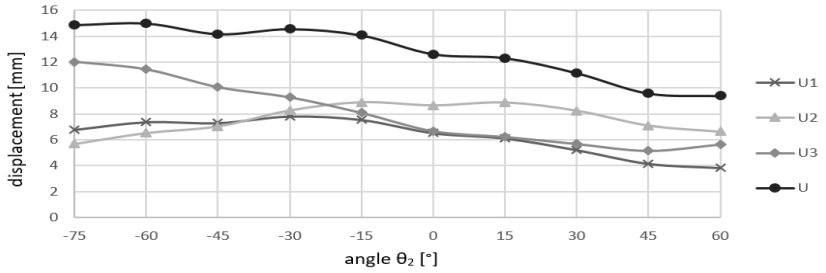

Fig. 10. Maximum displacement as a function of angle θ_2: U1 – displacement along the axis transverse to the walking direction (axis *x* in Fig. 1), U2 – displacement along the vertical axis (axis *z* in Fig. 1), U3 – displacement along the axis parallel to the walking direction (axis *y* in Fig. 1), U – resultant displacement

Based on the stress values from the graph in Fig. 11 we can see that the stress values for negative angles are slightly higher than for positive angles. With much smaller differences their effect can be expected to be considerably smaller, as compared to the effect of the above-described displacements. Note a rapid increase in the stress values for negative angles greater than –60°. This can indicate high loads in the area of the distal link drive, which can lead to the drive system overload. Hence it is recommended to avoid such high values of negative angles.

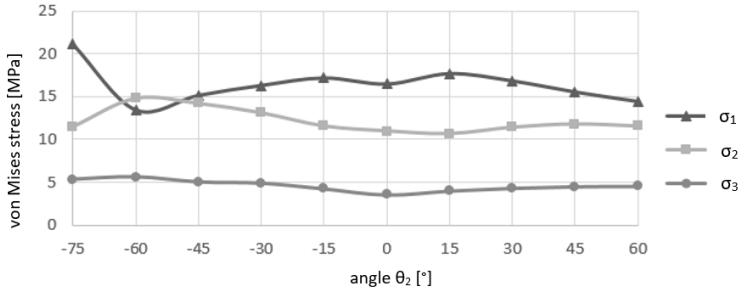

Fig. 11. Equivalent von Mises Stress vs. angle θ_2 at points No. 1, 2, 3

5. CONCLUSIONS

The robot posture at negative values of angle θ_2 is less favourable than the posture at positive angle in terms of strength and rigidity. For this reason, the walking robot should be controlled to obtain low position whenever possible and clearance should be increased only when there is a risk of contact with the ground. This will have a good effect also on the stability of movement. The part most prone to the occurrence of high stresses is the middle part of the leg (femur) and, as such, it deserves particular attention when designing the walking robot leg.

REFERENCES

Friedrich P, Zielińska T., Walking: biological and technological aspects, Springer-Verlag, Wiedeń 2004.

Lewinger W.A, Branicky M.S., Quinn R.D., Insect-inspired, actively compliant hexapod capable of object manipulation, [in:] Climbing and Walking Robots: Proceedings of 8th International Conference on Climbing and Walking Robots and the Support Technologies for Mobile Machines (CLAWAR 2005), p. 65–72.

Morecki A., Knapczyk.J, Podstawy robotyki – teoria i elementy manipulatorów i robotów, wyd 3, Warszawa 1999.

Wojtkowiak D., Projekt koncepcyjny robota kroczącego wzorowanego na budowie owada, praca magisterska, Politechnika Poznańska, Poznań 2015.

Zielińska T., Maszyny kroczące – Podstawy, projektowanie, sterowanie i wzorce biologiczne, wyd. 2, PWN, Warszawa 2014.

KOMPUTEROWA ANALIZA KONSTRUKCJI NOGI ROBOTA KROCZĄCEGO WZOROWANEGO NA BUDOWIE OWADA – CZ. 1 – ANALIZA STATYCZNA MES

Streszczenie

Niniejszy artykuł ma na celu przedstawienie zależności pomiędzy obciążeniem nogi, a sylwetką robota kroczącego wzorowanego na budowie owada, określonej na podstawie komputerowych badań symulacyjnych. W artykule zaprezentowano wyniki statycznej analizy MES modelu 3D pedipulatora wykonanej w programie Abaqus 6.13. Dodatkowo w artykule przedstawiono strukturę kinematyczną robota kroczącego wzorowanego na budowie owada z możliwością manipulacji obiektami.

Słowa kluczowe: robot kroczący, maszyna krocząca, hexapod, quadruped, pedipulator